Measurement of Nitrided SiO_2/Si Interface Roughness by Crystal-Truncation Rod Profiling

J.L. Jordan-Sweet and R. Ludeke
IBM Research Division, P.O. Box 218, Yorktown Heights, NY 10598,
T.B. Hook
IBM Microelectronics Division, Essex Junction, VT 05452,
and
K.W. Evans-Lutterodt
Bell Laboratories, Lucent Technologies, Murray Hill, NJ 07974

Abstract

The technique of crystal-truncation rod (CTR) profiling has been used to measure the interface roughness of nitrided gate oxides on Si(001). If an overlayer is truly amorphous, the variation of intensity along the truncation rods yields information about the rms roughness of the interface between the crystal substrate and the layer. CTR profiling is a non-destructive probe that can measure interface roughness with statistical meaning over a large dynamical range of scale. Although diffraction from the buried interface is orders of magnitude weaker than that from the bulk wafer, it can be measured easily using synchrotron radiation. This paper describes how the technique is applied to the case of ultrathin SiO_2 and nitrided SiO_2 on Si(001). Results are presented for a variety of oxidation processes, and the strengths and shortcomings of the technique are discussed.

Introduction

As increasing numbers of microelectronic devices are crowded onto chips in each generation to lower their cost and increase their speed, the areas of individual features in each device, such as contacts, gates, metal lines, and dielectric layers, continue to shrink. The preservation of reasonable aspect ratios forces them also to become extremely thin. In the current generation of Complementary Metal Oxide Semiconductor (CMOS) devices, the gate dielectric is about 45Å thick. By the year 2006, this could reach 15-20Å[1]. Figure 1 shows a cartoon of a Metal Oxide Semiconductor Field Effect Transistor (MOSFET). The carrier channel consists of doped single-crystal silicon and is that part of the transistor where current passes between the source and drain when voltage is applied to the gate. High charge-carrier mobility is one of the goals of FET design, and it can be compromised by carrier scattering from defects near the SiO_2/Si interface, or from the interface itself, if it is rough[2]. Also, the quality of the gate dielectric affects such parameters as charge-to-breakdown, dopant diffusion, interface states, and fixed charge[3]. The dielectric must be uniform in thickness, have few defects, have a very smooth interface, tie up as many dangling Si bonds as possible at the interface, and have very low strain.

Copyright (C) JCPDS-International Centre for Diffraction Data 1999

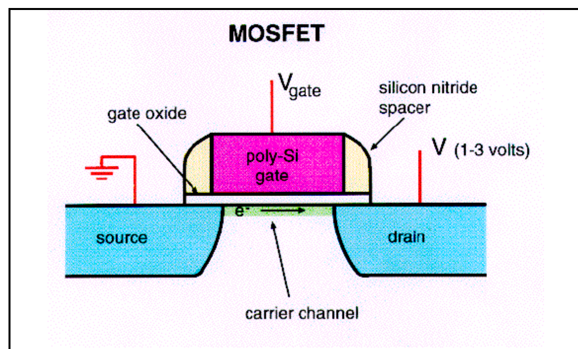

Currently, the material of choice for gate dielectrics is SiO_2. A number of exotic materials such as aerogels and polyimides are being evaluated for devices far into the future[4], but improvements continue to be made to SiO_2. Among those recently reported is wet oxidation, where the addition of water vapor during oxidation reduces the problem of low-voltage breakdowns[5]. It also has been found that the addition of nitrogen to the oxidation or post-oxidation annealing step improves many of the electrical characteristics of a device. Nitrogen is introduced in the form of NH_3, N_2, NO, or N_2O. Improvements attributed to nitridation include increased charge-to-breakdown[6-8], decreased boron diffusion[9,10], lower interface state density[6], less charge trapping[6], increased immunity to hot carrier damage[11,12], and reduced strain at the interface[13]. Auger Electron Spectroscopy[14] and Secondary Ion Mass Spectroscopy[6] have shown that nitrogen-rich regions are located at the Si/SiO_2 interface and at the top surface of the oxide layer. Subsequent re-annealing or rapid thermal annealing of either SiO_2 or nitrided SiO_2 further improves the electrical characteristics[6,7,15].

In this paper we present results of studies to determine the roughness of the Si/SiO_2 interface as a function of oxide processing parameters, including a range of nitridation conditions, annealing temperatures, and gas pressures. The samples measured are listed in Table 1.

Sample #	Description	t (Å)
0	Native oxide	
1	DWD 800EC	70
2	DWD 800EC, N_2/O_2 anneal 850EC	72
3	DWD 800EC, N_2O anneal 950EC	70
4	DWD 800EC, N_2 anneal 950EC	72
5	DWD 800EC, N_2/O_2 anneal 950EC	72
7	Dry O_2 900EC	70
9	“hipox” 800EC 10atm O_2	70
10	“hipox” 800EC 20atm N_2O	70
11	“hipox” 800EC 15atm N_2O	70
13	DWD 800EC, N_2O anneal 950EC	70

Table 1: List of samples measured by CTR profiling. DWD is dry-wet-dry oxidation. “hipox” is high-pressure oxidation.

Variations of standard techniques such as specular reflectivity, ellipsometry, atomic force microscopy (AFM), and transmission electron microscopy (TEM) have been applied to the study of SiO_2/Si interface roughness and dielectric thin film structure. Some of these, such as reflectivity and ellipsometry, rely heavily upon the ability to model the film accurately. These two techniques also have parameters that are hard to deconvolve, such as thickness, density and roughness[16]. "Difference reflectivity" has been used[17,18] to measure a dense layer in ultrathin thermal gate oxides and also the structural relaxation and flattening of the SiO_2/Si interface during annealing. Off-specular, or diffuse, scattering can distinguish between roughness and density, as well as determine lateral correlations (the spatial frequency spectrum) of the interface roughness, but to our knowledge it has not been applied to this system. Ellipsometery is a fast, nondestructive technique for measuring film roughness, but accurate angles are difficult to measure, and in its standard use it is not sensitive to buried interfaces. However, Liu *et al.*[19] have used "spectroscopic immersion ellipsometry", where the sample is measured in a liquid which matches the refractive index of the layer, to study thickness and substrate orientation effects on the width of the sub-oxide interface layer and interface roughness. The techniques of AFM and TEM involve destructive sample preparation (removal of oxide layer or thinning of the entire sample) and are microscopic probes that do not give a statistical sampling of the interface roughness; however, they are direct measurements that don't rely on models. It is assumed that removal of the oxide layer does not affect the surface morphology. AFM also is not sensitive to local fluctuations less than around 2nm, but it has the advantage of yielding lateral correlations, or frequency spectra, of roughness[2,16]. This can be important in assessing the effect of roughness on carrier mobility, since it has been demonstrated that long-wavelength roughness (longer than the electron mean-free path) has little influence on inversion layer mobility[2]. There are several studies that compare techniques, such as AFM and ellipsometry[16,19], or correlate structure with electrical measurements[2,13,14,20].

Crystal-Truncation Rod Profiles

Owing to the high flux provided by synchrotron radiation sources, it has been possible to probe the structure of buried interfaces non-destructively using x-rays. A recently developed x-ray diffraction technique, Crystal-Truncation Rod (CTR) scattering[21,22], has been applied to the study of structure in thin SiO_2 films[23-26], and to the roughness of the SiO_2/Si interface[27,28]. CTRs arise from the fact that diffraction from truncated crystals has a different signature than that from the bulk. X-ray diffraction measures the Fourier transform of the electron density. An infinitely extended perfect crystal gives rise to diffracted intensity at specific points in reciprocal space, with each Bragg point corresponding to diffraction from a set of planes formed by "sheets" of atoms separated by a distance d. A Bragg point is defined by *hkl*, which are the indices for those planes[29] (Figure 2a). If the crystal is truncated abruptly and smoothly, the "exposed" 2D plane of atoms at the surface produces rods of diffracted intensity normal to the surface (Figure 2b). Each rod has an index *hk*. The reciprocal space 3-D map is a superposition of rods along the K_z (or *l*) direction and the regular Bragg lattice (Figure 2c). If the truncated surface is rough, the intensity between Bragg points along the rod drops off rapidly (Figure 2d). The CTR indexed as 00 is a

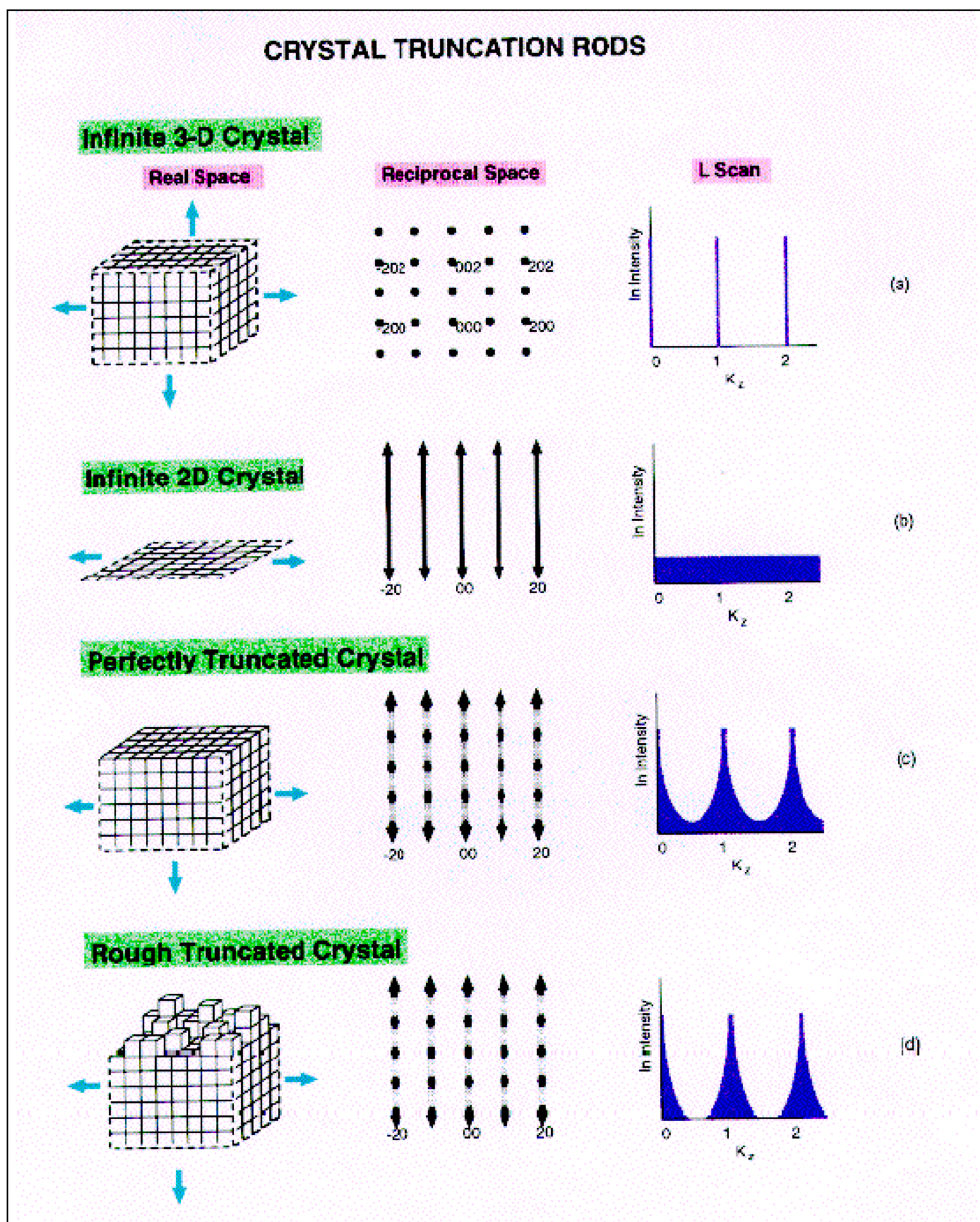

Figure 2 A schematic showing the real-space structure, reciprocal space map (projected into two dimensions), and intensity vs. Kz scans for an ideal a) infinite 3-D cubic crystal, b) infinite 2-D crystal, c) perfectly truncated 3-D cubic crystal, and d) roughly truncated 3-D crystal.

special case. It is the specular rod, and is the one scanned when specular reflectivity is measured. The specular rod will show oscillations due to Fresnel scattering if the overlayer film is smooth and uniform. It will also show asymmetry if there is any laminar order in the film, as was found by Rabedeau *et al.*[26] for room temperature dry oxides on Si(001) and by Robinson *et al.*[23] for thermal oxides on Si(111).

Assuming that the SiO_2 film is completely amorphous, we can follow the procedure developed by M-T Tang *et al.*[27] for modelling the roughness of the SiO_2/Si(001) interface and calculating the expected x-ray intensity along a truncation rod. They start with an infinite lattice of Bragg points in reciprocal space which are produced by diffraction from an infinite 3-D cubic crystal. The diffracted amplitude is:

$$\boldsymbol{r}(K) = \sum_{hkl} \boldsymbol{r}_0(K)\boldsymbol{d}\left(K - h\tfrac{2\boldsymbol{p}}{a}\hat{x} - k\tfrac{2\boldsymbol{p}}{a}\hat{y} - l\tfrac{2\boldsymbol{p}}{a}\hat{z}\right), \quad (1)$$

where $\boldsymbol{r}_0(K)$ is the atomic form factor, and a is the cubic lattice parameter. The infinite 3-D crystalline array is then convoluted with a termination function, g(z), which describes the truncated interface. They choose an error function having a width parameter λ, which has the form of the standard deviation of the Gaussian probability distribution. Below the center of the interface (z <0) there is also an attenuation factor, $e^{\mu z}$, that accounts for loss of intensity as the x-ray beam penetrates the sample. A perfectly flat surface corresponds to λ=0. As the interface width (roughness) increases, the parameter λ does also, and the termination function changes from a sharp step to one that is broadened and rounded-off. In the limit that $\boldsymbol{m} \longrightarrow 0$, for a discrete lattice, the diffracted intensity is

$$\left|\boldsymbol{r}(K)\right|^2 = \left|\boldsymbol{r}_0(K)\right|^2 \sum_{hk} \boldsymbol{d}\left(K - h\tfrac{2\boldsymbol{p}}{a}\hat{x} - k\tfrac{2\boldsymbol{p}}{a}\hat{y}\right)\frac{1}{\sin^2\left(\frac{K_z a}{2}\right)} \exp\left[-\boldsymbol{l}^2 \sin^2\left(\frac{K_z a}{2}\right)\right] \quad (2)$$

The integrated intensity of the CTR as a function of K_z is measured and fit to a numerical equivalent of Equation 2.

Experimental

Measurements were taken at Beamline X20A of the National Synchrotron Light Source at Brookhaven National Laboratory. 8.048 kV x-rays were focused onto a spot size of 1x1mm at the sample. Samples were mounted in a stress-free manner on a four-circle Huber diffractometer. A detector collected diffracted beam through 2x2mm slits at a distance of 848mm from the sample

for a 1.6mr acceptance angle. Integrated intensities were measured by taking theta scans across the ($00K_z$) and/or ($20K_z$) rods of the samples near the (004) and (202) bulk Bragg peaks, respectively. Typical peak intensities for the ($20K_z$) rod ranged from $1x10^5$ cps at K_z=2.05 reciprocal lattice units (r.l.u.) to 12 cps at K_z=2.7 r.l.u.. Background was approximately 78 cps. Each theta scan peak was numerically integrated, subtracting a background calculated by averaging the baseline of the scan. Integrated intensities from scans taken at equal $+K_z$ and $-K_z$ values from the bulk Bragg position were averaged to eliminate any influence from possible asymmetry due to substrate relaxation at the interface[27]. The plots of CTR intensities *vs.* K_z were then fit using a least-squares refinement routine and equation 2. A typical plot of data and the corresponding fitted curve is shown in Figure 3. The fit parameters consisted of an intensity and Gaussian width. The Gaussian width, l, was then multiplied by the Si lattice parameter, a = 5.431 Å, to obtain the interface width.

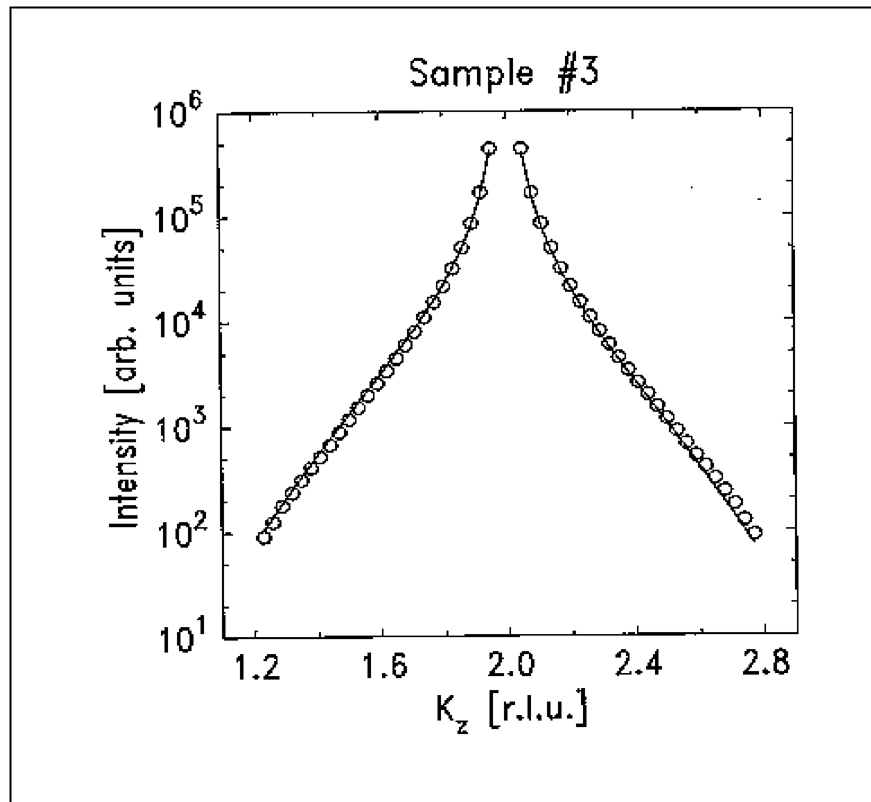

Figure 3 Typical plot of (20Kz) CTR data points around the bulk (202) Si reflection. This data is from Sample #3. The lines are fits to the data using a function based on Equation 2.

Results

Results of the fits are shown in Table 2. The most striking observation is that the interface widths obtained using the ($00K_z$) rod data are consistently higher than those obtained using the B($20K_z$) rod data. The fits to the ($00K_z$) rod data also were not as good. The data had to be truncated from the ends farthest from the (004) peak in order to obtain qualitatively acceptable fits (*i.e.* data from 3.6 to 4.4 r.l.u rather than from 3.5 to 4.5 r.l.u.). This is consistent with results from M.-T. Tang *et al.*[27]. for native and thermal oxides, and can be explained by other measurements that have detected a lamellar structure close to the interface in thin room temperature[26] and

Copyright (C) JCPDS-International Centre for Diffraction Data 1999

thermal[25] oxide films on Si(001) and thermal oxide films on Si(111)[23]. Because the ($00K_z$) rod is the specular rod, it

Sample #	Description	a×**l** (Å) ($00K_z$)	a×**l** (Å) ($20K_z$)
0	Native oxide	3.096	3.014
1	DWD 800EC	2.553	2.390
2a	DWD 800EC, N_2/O_2 anneal 850EC		1.591
2b	" " "		1.591
3	DWD 800EC, N_2O anneal 950EC		1.939
4	DWD 800EC, N_2 anneal 950EC		1.532
5a	DWD 800EC, N_2/O_2 anneal 950EC		1.532
5b	" " "		1.504
7	Dry O_2 900EC	2.390	2.015
9	"hipox" 800EC 10atm O_2	2.661	
10	"hipox" 800EC 20atm N_2O	2.770	
11	"hipox" 800EC 15atm N_2O		2.167
13	DWD 800EC, N_2O anneal 950EC	2.498	

Table 2: Results for samples measured by CTR profiling. λ ($00K_z$) is the interface width calculated by fitting the CTR in the vicinity of the (004) bulk reflection. λ ($20K_z$) is the interface width calculated by fitting the CTR in the vicinity of the (202) bulk reflection. Samples 2a and 2b, and 5a and 5 bare two different pieces taken from wafers #2 and #5, respectively.

is sensitive to any ordering in the z direction. Thus, one would expect any lamellar structure in the oxide film to add to the interface width of the ($00K_z$) data and not affect the off-specular ($20K_z$) data. Also noticeable is the grouping of interface widths into three sets of similar ranges: for samples 1, 3, and 7, around 2 Å; for samples 2, 4, and 5, around 1.55 Å; and for samples 9, 10, and 11, around 2.2-2.7 Å. The differences between these groups are greater than the differences among samples within the groups. Each of these three groups of samples were processed as batches at different times. Thus, processing conditions or substrate parameters such as miscut or doping can have more drastic effects on interface roughness than variations in oxidation processing alone. A more consistent set of samples is required to make a good comparison between various oxidation processes. Note that the reproducibility is quite good (samples 2a and b, and samples 5a and b). Also, the ($20K_z$) rods need to be measured for samples 9, 10, and 13. However, based on the results presented here, some remarks can be made. First, clearly, thermal oxidation produces a smoother interface than is measured on native oxide samples. This was noted by M.T. Tang *et al.*[27]. Secondly, comparing the ($20K_z$) results for samples 2, 4, and 5 shows that higher oxidation temperatures in nitrided oxides produce smoother interfaces, as has been reported also for plain thermal oxides[28]. Thirdly, in comparing samples 1, 3, and 7, one sees that sample 3 has a smoother interface than the other two, which were oxidized at lower temperatures. This result shows that

nitridation does not introduce any additional interface roughness. However, electrical measurements show that the electron mobility of the nitridized sample is lower that that of the pure oxides. Thus, we can conclude that this reduced mobility is *not* owed to any increased surface roughness. Finally, the high pressure process does not appear to present any improvements in interface roughness.

Conclusions

There are distinct advantages to using CTR profile measurements to determine interface roughness in SiO_2/Si systems. The technique is non-destructive. It yields a statistical average of roughness over the size of the x-ray spot (on the order of millimeters). A natural extension of this technique would be to use small x-ray beams to measure interface roughness in individual small structures, such as test structures or models of devices. One could expect to measure interface roughness over areas ranging from millimeters to microns. There are few parameters for fitting and no need to model the overlayer, provided that it is amorphous. No sample preparation is necessary and the measurements are made in ambient conditions. The measurements described here required only a few hours per sample to make. When one relies on a simple model, there are possible pitfalls to be aware of. Any lamellar structure (with no in-plane order) will affect the specular truncation rod. Any crystalline structure in the overlayer will affect other rods as well. The background can have asymmetries if there are lateral correlations in the interface roughness (just as one sees in diffuse specular reflectivity). Finally, miscut in the substrate can produce steps which can either add to the interface roughness or tilt the CTR[27].

The results presented show that consistent substrate qualities and sample processing are vital to a systematic study of SiO_2/Si interface roughness. The striking differences in interface roughness between sets of samples processed at different times could be due to variations in substrate miscut, doping or cleaning procedures, or other processing steps. It was also found that off-specular rods are required for accurate roughness measurements because of lamellar structure in the oxide layer near the interface. The smoothest interfaces were those where the oxide was processed at higher temperatures in dry-wet-dry conditions. No striking improvements were found for the nitridized samples or samples processed under pressure. A more complete and consistent set of samples is required for further understanding.

Acknowledgements

The x-ray diffraction experiments was performed at the IBM/MIT beamline X20 at the National Synchrotron Light Source, Brookhaven National Laboratory, which is supported by DOE contract DE-AC02-76CH00016. The high-pressure oxidations were done at GaSonics International, San Jose, CA.

References

1. National Technology Roadmap for Semiconductors, Semiconductor Industry Association.

2. T. Yamanaka, S.J. Fang, H-C Lin, J.P. Snyder, and C. R. Helms, IEEE Electron. Dev. Lett. 17, 178 (1996).

3. M. M. Moslehi and K.C. Saraswat, IEEE Trans. Electron. Devices ED-32, 106 (1985).

4. Solid State Technology.

5. D.J. DiMaria, pvt. communication.

6. H. Hwang, W. Ting, B. Maiti, D-L Kwong, and J. Lee, Appl. Phys. Lett. 57, 1010 (1990).

7. Y-L Wu and J-G Hwu, J. Vac. Sci. Technol. B 12, 2400 (1994).

8. T. Ito, T. Nakamura, and H. Ishikawa, IEEE Trans. Electron. Devices, ED-29, 498 (1982).

9. H. Fang, K.S. Krisch, B.J. Gross, C. Sodini, J. Chung, and D. Antoniadis, Electron. Dev. Lett. 13, 217 (1992).

10. L. Han, D. Wristers, M. Bhat, and D. Kwong, Electron. Dev. Lett. 16, 319 (1995).

11. T. Matsuoka, S. Taguchi, H. Ohtsuka, K. Taniguchi, C. Hamaguchi, S. Kakimoto, and K. Uda, IEEE Trans. on Electron. Devices, 43, 1364 (1996).

12. T.B. Hook, K. Watson, E. Lee, D. Martin, R. Ganesh, S. Kim, and A. Ray, IEEE Electron. Dev. Lett. 18, 471 (1997).

13. R.P. Vasquez and A. Madhukar, Appl. Phys. Lett. 47, 998 (1985).

14. T. Hori, H. Iwasaki, and K. Tsuji, IEEE Trans. Electron. Dev. 36, 340 (1989).

15. X. Chen and J.M. Gibson, Appl. Phys. Lett. 70, 1462 (1997).

16. S.J. Fang, W. Chen, T. Yamanaka, and C.R. Helms, Appl. Phys. Lett. 68, 2837 (1996).

17. N.Awaji, S. Ohkubo, T. Nakanishi, Y. Sugita, K. Takasaki, and S. Komiya, Jpn. J. Appl. Phys. 35, L67 (1996).

18. N.Awaji, Satoshi Ohkubo, T. Nakanishi, K. Takasaki, and S. Komiya, Appl. Surf. Sci. (1996/7).

19. Q. Liu, J.F. Wall, and E.A. Irene, J. Vac. Sci. Technol. A12, 2625 (1994).

20. P.O. Hahn and M. Henzler, J. Vac. Sci. Technol. A2, 574 (1984).

21. S.R. Andrews and R.A. Cowley, J. Phys. C: Sol. State Phys. 18, 6427 (1985).

22. I.K. Robinson, Phys. Rev. B 33, 3830 (1986).

23. I.K. Robinson, W.K. Waskiewicz, R.T. Tung, and J. Bohr, Phys. Rev. Lett. 57, 2714 (1986).

24. T.A. Rabedeau, I.M. Tidswell, P.S. Pershan, J. Bevk, and B.S. Freer, Appl. Phys. Lett. 59, 706 (1991).

25. Y. Iida, T. Shimura, J. Harada, S. Samata, and Y. Matsushita, Surf. Sci. 258, 235 (1991).

26. T.A. Rabedeau, I.M. Tidswell, P.S. Pershan, J. Bevk, and B.S. Freer, Appl. Phys. Lett. 59, 3422 (1991).

27. M-T Tang, K.W. Evans-Lutterodt, G.S. Higashi, and T. Boone, Appl. Phys. Lett. 62, 3144 (1993).

28. M-T. Tang, K.W. Evans-Lutterodt, M.L. Green, D. Brasen, K. Krisch, L. Manchanda, G.S. Higashi, and T. Boone,Appl. Phys. Lett. 64, 748 (1994).

29. B.D. Cullity, Elements of X-ray Diffraction, 2nd ed. (Addison-Wesley, Reading, MA) 1978, pp.42-47.